ACS chemical biology

pubs.acs.org/acschemicalbiology

Articles

Screen for Modulation of Nucleocapsid Protein Condensation Identifies Small Molecules with Anti-Coronavirus Activity

Rui Tong Quek, Kierra S. Hardy, Stephen G. Walker, Dan T. Nguyen, Taciani de Almeida Magalhães, Adrian Salic, Sujatha M. Gopalakrishnan, Pamela A. Silver,* and Timothy J. Mitchison*

Cite This: *ACS Chem. Biol.* 2023, 18, 583−594

Read Online

ACCESS | Metrics & More | Article Recommendations | Supporting Information

ABSTRACT: Biomolecular condensates formed by liquid−liquid phase separation have been implicated in multiple diseases. Modulation of condensate dynamics by small molecules has therapeutic potential, but so far, few condensate modulators have been disclosed. The SARS-CoV-2 nucleocapsid (N) protein forms phase-separated condensates that are hypothesized to play critical roles in viral replication, transcription, and packaging, suggesting that N condensation modulators might have anti-coronavirus activity across multiple strains and species. Here, we show that N proteins from all seven human coronaviruses (HCoVs) vary in their tendency to undergo phase separation when expressed in human lung epithelial cells. We developed a cell-based high-content screening platform and identified small molecules that both promote and inhibit condensation of SARS-CoV-2 N. Interestingly, these host-targeted small molecules exhibited condensate-modulatory effects across all HCoV Ns. Some have also been reported to exhibit antiviral activity against SARS-CoV-2, HCoV-OC43, and HCoV-229E viral infections in cell culture. Our work reveals that the assembly dynamics of N condensates can be regulated by small molecules with therapeutic potential. Our approach allows for screening based on viral genome sequences alone and might enable rapid paths to drug discovery with value for confronting future pandemics.

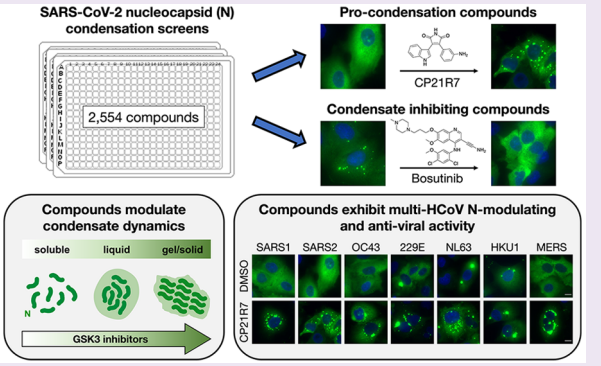

INTRODUCTION

Biomolecular condensates are membrane-less organelles formed by liquid−liquid phase separation of specific RNAs and/or proteins, resulting in their local concentration in a liquid-like compartment distinct in constituents from the surrounding cytoplasm or nucleoplasm.[1−3] Such biomolecular condensates have been implicated in the formation of signaling complexes, processing bodies, stress granules (SGs), and germline bodies,[1] where they facilitate the segregation and concentration of factors involved in various cellular processes. The material properties of condensates are tailored to their functions; dynamic condensates with mobile constituents enhance biochemical reactions that involve molecular turnover, whereas more glasslike or solid condensates promote stiffness for structural support.[4]

Phase separation and the formation of liquid condensates known as viroplasms or inclusion bodies have been observed in large groups of viruses such as the Mononegavirales order of nonsegmented negative-strand RNA viruses[5−13] and the Reoviridae family of double-stranded RNA viruses.[14] The formation of viroplasms is induced by viral proteins and RNAs expressed during infection, and they serve as organizational hubs for the concentration of viral or host factors involved in viral entry, replication, virion assembly, and/or packaging.[15] The SARS-CoV-2 nucleocapsid (N) protein drives virion packaging through RNA binding and enhances viral transcription and replication at replication and transcription complexes (RTCs).[16,17] Recent observations that the SARS-CoV-2 N protein forms liquid condensates[16,18−24] has raised the possibility that these N condensates may also behave as dynamic viroplasms. However, whether condensate assembly is a conserved property of HCoV Ns has not been examined.

Macromolecular phase separation is often driven by unstructured regions of proteins, which makes condensates unconventional for targeting by small-molecule drugs. Nevertheless, recent studies successfully identified small molecules that modulate phase transitions of proteins involved in amyotrophic lateral sclerosis (ALS)[25,26] and respiratory syncytial virus (RSV) infection.[27] These studies, as well as the recent founding of condensate-focused biotechnology companies, have led to an explosion of interest in targeting condensates for drug discovery, but to date, few active molecules have been disclosed.[28−30] In principle, small

Received: December 13, 2022
Accepted: February 3, 2023
Published: February 16, 2023

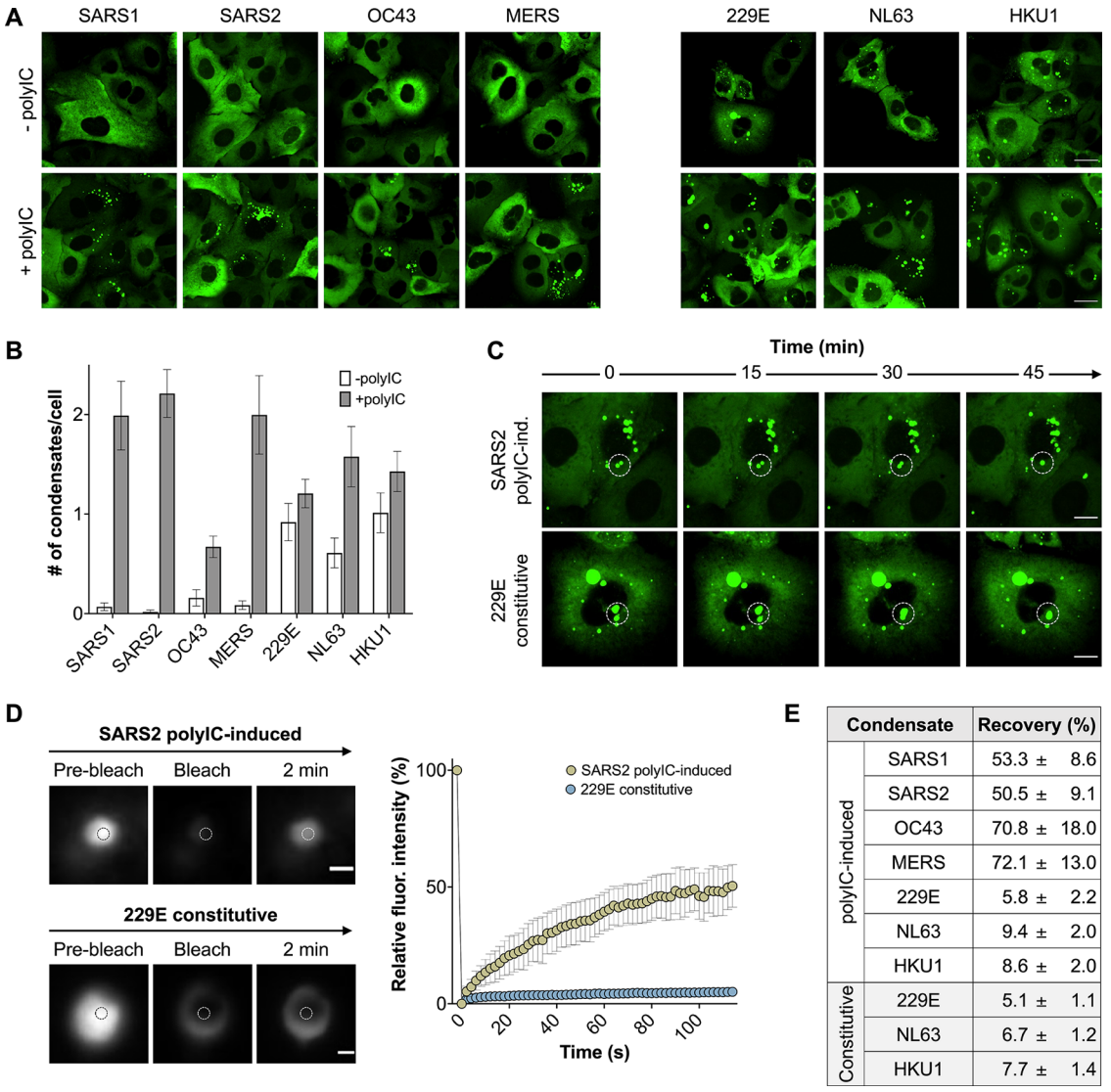

Condensate		Recovery (%)
polyIC-induced	SARS1	53.3 ± 8.6
	SARS2	50.5 ± 9.1
	OC43	70.8 ± 18.0
	MERS	72.1 ± 13.0
	229E	5.8 ± 2.2
	NL63	9.4 ± 2.0
	HKU1	8.6 ± 2.0
Constitutive	229E	5.1 ± 1.1
	NL63	6.7 ± 1.2
	HKU1	7.7 ± 1.4

Figure 1. HCoV N proteins phase-separate in a polyIC-inducible manner. (A) Fluorescence images of A549 cells stably expressing N from the seven HCoVs. Images taken at 40× air magnification, confocal. Scale bar, 20 μm. SARS1: SARS-CoV; SARS2: SARS-CoV-2; OC43: HCoV-OC43; 229E: HCoV-229E; NL63: HCoV-NL63; HKU1: HCoV-HKU1; MERS: MERS-CoV. (B) Quantification of number of N condensates per cell for each of the seven cell lines. (C) Time-lapse imaging showing polyIC-induced SARS-CoV-2 and constitutive HCoV-229E N condensate fusion events over time. Scale bar, 10 μm. ind.: induced. (D) Fluorescence recovery after photobleaching (FRAP) analyses of SARS-CoV-2 polyIC-induced and HCoV-229E constitutive N condensates. Mean fluorescence intensity plot illustrates FRAP results for $n = 7$ condensates per condition. Scale bar, 1 μm. fluor: fluorescence. (E) Final fluorescence recovery percentage 2 min post-bleach.

molecules could achieve therapeutic activity by inhibiting the assembly of cytotoxic condensates[25,26] or by promoting condensation, leading to hardening and cessation of essential dynamics.[27] Given the ongoing need for antivirals to confront the COVID-19 pandemic, and the likelihood that similar pandemics will emerge in the future, we focused on identifying small molecules that perturb SARS-CoV-2 N condensation, with the hope that some might exhibit broad-spectrum antiviral activity. We developed a cell-based high-content screening platform to identify small molecules that either promote or inhibit N condensation and identified small molecules with condensate-modulating activity. Our results suggest it may be possible to discover drug-like small molecules that promote and inhibit condensation of many proteins and RNAs, which will open new paths to drug discovery.

RESULTS AND DISCUSSION

HCoV N Condensates Are PolyIC-Inducible and Exhibit Varied Material Properties. To investigate the condensation behavior of HCoV N proteins, we stably expressed each of the seven HCoV N proteins fused to a C-terminal EGFP in A549 cells (human lung cancer-derived) (Figure 1A and Table S1). Western blots confirmed that the expression levels of each of the seven N proteins were similar among the stably expressing A549 cells (Figure S1A). Under control conditions, SARS-CoV, SARS-CoV-2, HCoV-OC43, and MERS-CoV N showed diffuse cytoplasmic localization, while HCoV-229E, HCoV-NL63, and HCoV-HKU1 N formed spherical condensates (henceforth referred to as "constitutive" condensates) of varying numbers (Figure 1A,B). Thus, the tendency to phase-separate and condense varies between N species under these conditions.

https://doi.org/10.1021/acschembio.2c00908
ACS Chem. Biol. 2023, 18, 583−594

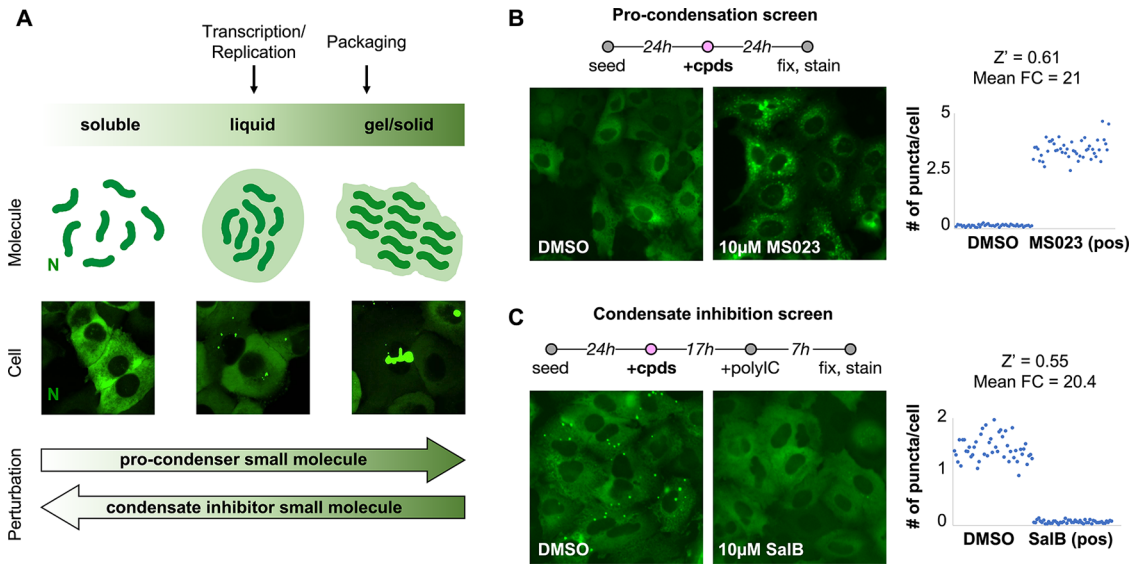

Figure 2. High-content phenotypic screening assay to identify modulators of SARS-CoV-2 N condensation. (A) Schematic illustrating the sliding scale of N condensate material properties, adapted with permission from Boeynaems, S.; Alberti, S.; Fawzi, N. L.; Mittag, T.; Polymenidou, M.; Rousseau, F.; Schymkowitz, J.; Shorter, J.; Wolozin, B.; Van Den Bosch, L.; Tompa, P.; Fuxreiter, M. Protein Phase Separation: A New Phase in Cell Biology, Trends Cell Biol. **2018**, *28*, 420−435, Copyright 2018 Elsevier. N can exist in a soluble, diffuse cytoplasmic state, or anywhere along a continuum ranging from liquid-like condensates to more solid gel-like states. Intermolecular interaction strength tunes the material properties of condensates. On a cellular level, liquid-like condensates appear as small spherical puncta, while progression to more gel-like states may result in the formation of larger, more irregularly shaped aggregates. Small molecules that perturb the material state of N are referred to in this study as "pro-condensers" and "condensate inhibitors." (B) Schematic illustrating the pipeline for the pro-condensation screen to identify N condensation-inducing compounds. Representative images show the negative (dimethyl sulfoxide (DMSO)) and positive (10 μM MS023) controls. FC: fold change; pos: positive control. (C) Schematic illustrating the pipeline for the N condensate inhibition screen to identify N condensate-inhibiting compounds. Representative images show the negative (DMSO) and positive (10 μM salvianolic acid B) controls.

Upon transfection of low-molecular-weight polyinosinic−polycytidylic acid (polyIC), a synthetic analogue of dsRNA that mimics viral genome replication intermediates and triggers innate immune pathways, N condensates formed across all seven HCoV N cell lines (Figure 1A,B). For the species that exhibited constitutive condensation, the number of condensates increased upon polyIC transfection (Figure 1A,B). The addition of polyIC to an A549 cell line stably expressing EGFP alone did not result in condensate formation, confirming the essentiality of N for polyIC-induced condensate formation (Figure S1B). Across all seven Ns, both constitutive and polyIC-induced condensates exhibited flow and fusion/coalescence over time (Figures 1C and S1C), which are behaviors consistent with liquid−liquid phase separation. We also probed the dynamics of the various N condensates by monitoring fluorescence recovery after photobleaching (FRAP). PolyIC-induced SARS-CoV/SARS-CoV-2/HCoV-OC43/MERS-CoV N condensates were much more dynamic than constitutive HCoV-229E/HCoV-NL63/HCoV-HKU1 condensates, exhibiting faster and more complete recovery of fluorescence after photobleaching (Figures 1D,E and S1D). Moreover, polyIC-induced HCoV-OC43/MERS-CoV N condensates displayed faster dynamics than polyIC-induced SARS-CoV/SARS-CoV-2 N condensates (Figures 1E and S1D). Overall, the seven HCoV N proteins exhibit varied basal phase separation propensities with constitutive condensates being less dynamic than polyIC-induced condensates, and in all cases, polyIC increased N condensation.

To gain insight into the specific regions of N that contribute to differences in basal phase separation behavior between species, we expressed "domain swap" mutants of the SARS-CoV-2 and HCoV-229E N proteins in cells (Figure S1E). We observed that individually replacing the SARS-CoV-2 N protein N-terminal domain (NTD) and central Ser/Arg (SR)-rich linker domains with the equivalent domains from HCoV-229E N resulted in a significant increase in basal phase separation propensity. In addition, protein disorder prediction system (PrDOS) analyses[31] for all seven N proteins identified an approximately 25 amino acid region within the NTD with varying disorder prediction scores (Figure S1F), with N proteins that form constitutive condensates having lower predicted disorder scores compared to the N proteins with polyIC-inducible condensates. All in all, this suggests that differences in the properties of both the NTD and linker domains may explain the varied basal phase separation between the two N proteins.

High-Content Phenotypic Screening for Modulators of SARS-CoV-2 N Condensation. We hypothesized that modulating the phase behavior of SARS-CoV-2 N with small molecules may exert antiviral effects by perturbing the finely tuned dynamics of N condensates required for various stages of viral replication (Figure 2A). To identify compounds that promote or inhibit condensation of SARS-CoV-2 N, we devised two parallel screens (Figure 2B,C and Table S2). Briefly, to identify compounds that promote N condensation (henceforth referred to as pro-condensers), A549 cells stably expressing SARS-CoV-2 N-EGFP were treated with 10 μM compounds for 24 h (Figure 2B). To identify condensate inhibitors, 17 h after compound addition, cells were treated with polyIC for 7 h (Figure 2C). After fixing and staining, cells were imaged at 20× magnification and the number of N puncta per cell was scored by image analysis (Figure S2A). Positive control compounds were MS023, a type I protein arginine methyltransferase inhibitor known to induce N condensa-

https://doi.org/10.1021/acschembio.2c00908
ACS Chem. Biol. 2023, 18, 583−594

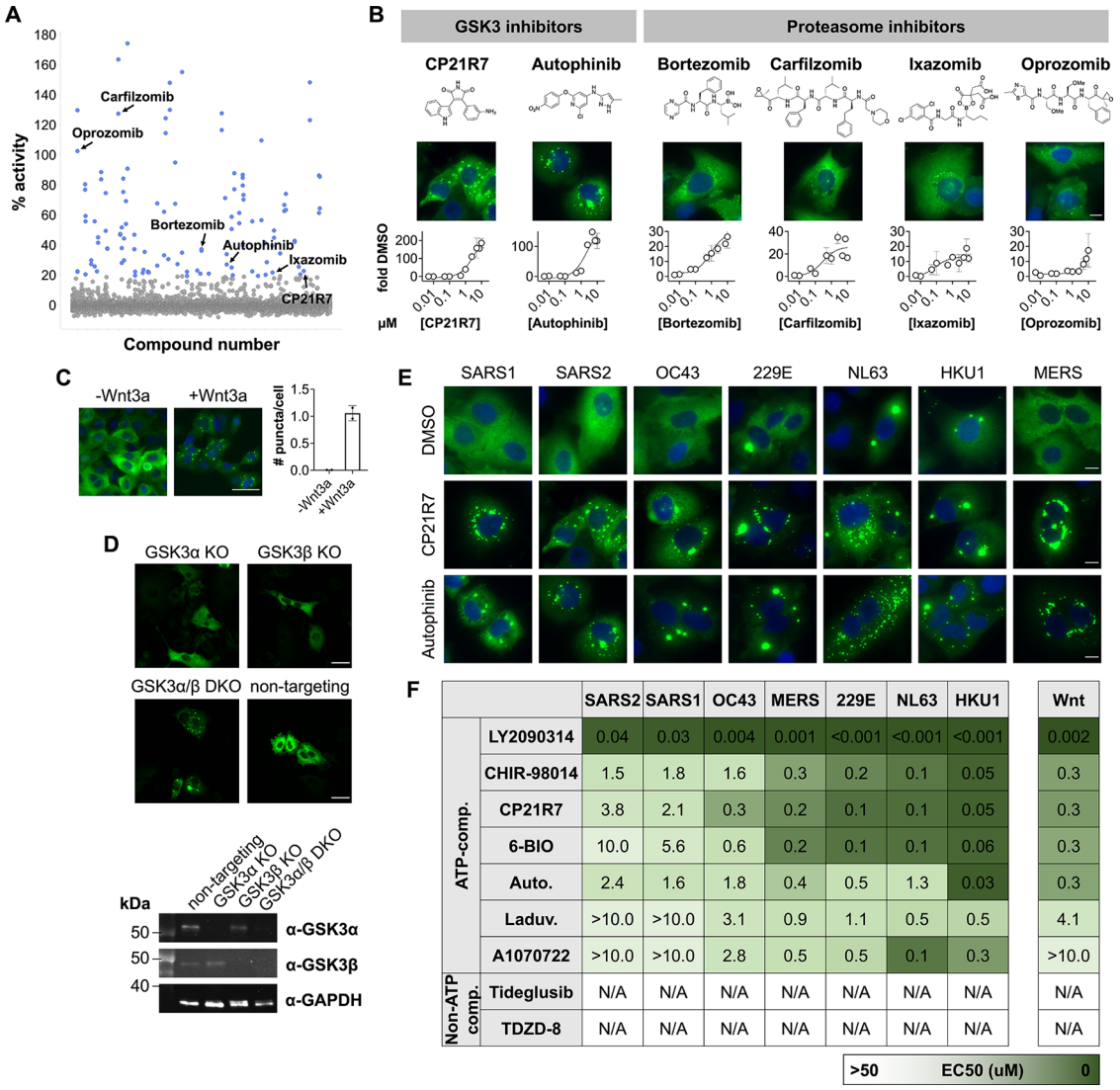

Figure 3. GSK3 and proteasome inhibitors promote pan-HCoV N condensation and condensate hardening. (A) Scatter plot illustrating SARS-CoV-2 N pro-condensation screening results. Data are represented as percentage N condensation activity over DMSO (% activity). Blue points: identified "pick" compounds. Validated hit compounds are annotated on the plot. (B) Hit compounds classified according to their annotated cellular targets. Dose−response curves indicate fold change in number of N puncta per cell over DMSO control (fold DMSO). Scale bar, 10 μm. (C) Fluorescence images and quantification for A549 SARS-CoV-2 N-EGFP cell lines treated with Wnt3a. Scale bar, 20 μm. (D) Fluorescence images and western blot quantification for GSK3α, GSK3β, and GSK3α/β CRISPR knockout cell lines illustrating increase in N condensation. Scale bar, 20 μm. Non-targeting: nontargeting sgRNA control; DKO: double knockout. (E) Representative fluorescence images of all seven HCoV N-EGFP cell lines treated with 10 μM GSK3 inhibitor hit compounds. Scale bar, 10 μm. (F) Left: N condensation EC50s for all seven HCoV N-EGFP cell lines across all GSK3 inhibitors. Right: Wnt signaling EC50s for all seven HCoV N-EGFP cell lines across all GSK3 inhibitors. Auto.: autophinib; Laduv.: laduviglusib.

tion,[32] and salvianolic acid B (SalB), a natural product identified in our pilot screen that robustly inhibited the formation of polyIC-induced condensates. The Z' values for the pro-condensation and condensate inhibition screening modalities were 0.61 and 0.55, respectively. We performed both screening modalities against the FDA-annotated Drug Library from Selleckchem (Selleck 2019) comprising 2554 compounds at 10 μM in technical duplicate, with two biological replicates. This was followed by confirmation of compounds in dose−response experiments with both the original screening assay (Figure S2A) and separate follow-up experiments with an independent image analysis pipeline (Figure S2B).

SARS-CoV-2 N Pro-Condensation Screen Identifies GSK3 and Proteasome Inhibitors. After counter-screening to remove fluorescent artifacts, cytotoxic hits, and compounds that act directly on EGFP, we identified six hit compounds that robustly increase the number of N puncta per cell (Figure 3A,B and Table S3). These fell into two classes by annotation and follow-up: inhibitors of the proteasomal catalytic core complex and GSK3 inhibitors. Proteasome inhibition could prevent N turnover, thereby increasing the concentration of N in cells and promoting its phase separation. However, we also observed an increase in N nuclear localization upon treatment of cells with the proteasome inhibitors (Figure S3A), suggesting that these small molecules may exert modulatory effects on N condensation through multiple mechanisms. Proteasome inhibition for cancer treatment has toxic side effects which preclude this target for antiviral drugs, so this hit class was not pursued further.

https://doi.org/10.1021/acschembio.2c00908
ACS Chem. Biol. 2023, 18, 583−594

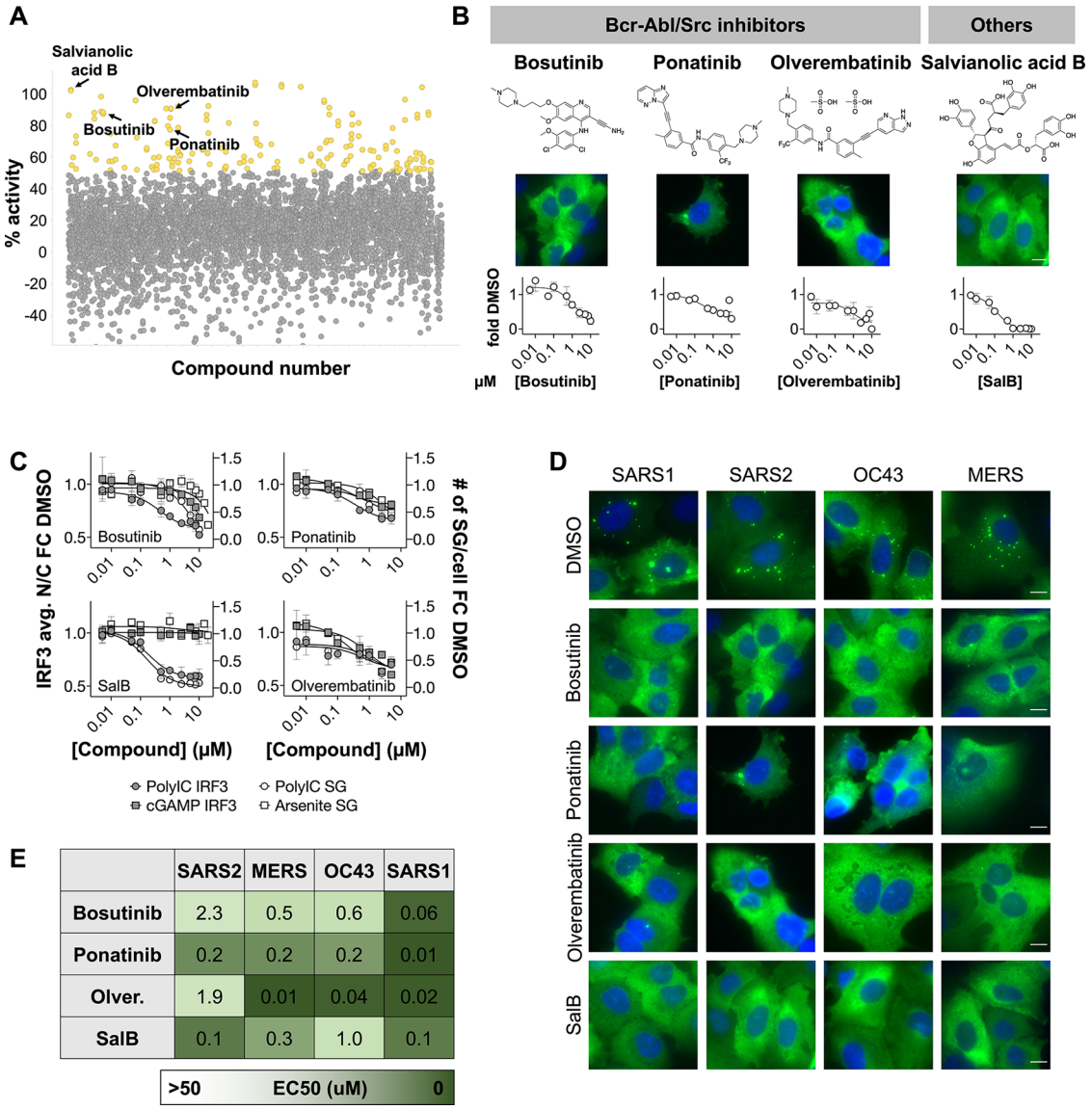

Figure 4. Diverse classes of compounds inhibit SARS-CoV-2 polyIC-induced N condensation. (A) Scatter plot illustrating SARS-CoV-2 N condensate inhibition screening results. Data are represented as percentage N condensate inhibition activity over DMSO (% activity). Yellow points: identified "pick" compounds. Validated hit compounds are annotated on the plot. (B) Hit compounds classified according to their annotated cellular targets. Dose−response curves indicate fold change of number of N puncta per cell over DMSO control (fold DMSO). Scale bar, 10 μm. (C) Dose−response curves illustrating inhibition of stress granule formation and IRF3 activation by various N condensate inhibitors. avg. N/C: average nuclear-to-cytoplasmic ratio; FC DMSO: fold change over DMSO. (D) Representative fluorescence images of SARS-CoV, SARS-CoV-2, HCoV-OC43, and MERS-CoV N-EGFP cell lines treated with 10 μM condensate inhibitors followed by transfected polyIC treatment. Scale bar, 10 μm. (E) N condensate inhibition IC50s for SARS-CoV, SARS-CoV-2, HCoV-OC43, and MERS-CoV N-EGFP cell lines across all four active condensate inhibitors. Olver.: olverembatinib; SalB: salvianolic acid B.

We identified one ATP-competitive GSK3 inhibitor (CP21R7) as a pro-condenser hit (Figure 3B). Autophinib, a second pro-condenser hit originally annotated as a VPS34 ATP-competitive inhibitor of autophagy, robustly induced N condensation and was later found to be a GSK3 inhibitor (see below). We therefore tested five other ATP-competitive GSK3 inhibitors (6-BIO, laduviglusib, A1070722, CHIR-98014, LY2090314) as well as the Mg^{2+}-competitive GSK3 inhibitor lithium chloride (LiCl) and found them to also induce N condensation, albeit with varying EC50s that spanned several orders of magnitude, with the most potent compound being LY2090314 (Figure S3B,C). Mass spectrometry analysis of N phosphorylation upon 1 μM LY2090314 treatment confirmed inhibition of phosphorylation predominantly at the start of the SR-rich region of the LKR domain as well as at four other minor phosphorylation sites within the disordered N- and C-terminal arms and the N-terminal RNA-binding domain (Figure S3D). Conversely, 1 μM CP21R7 inhibited phosphorylation of N to a smaller extent, consistent with the different EC50s and N condensation potencies for these two small molecules.

To test if GSK3 is indeed the relevant target of the pro-condenser compounds, we pursued gain- and loss-of-function experiments. We observed robust SARS-CoV-2 N condensation when cells were stimulated with Wnt3a ligand, which activates the Wnt signaling pathway and leads to GSK3 inhibition (Figure 3C). CRISPR-knockouts of GSK3α/β recapitulated the effect of inhibitors, with CRISPR-knockouts

https://doi.org/10.1021/acschembio.2c00908
ACS Chem. Biol. 2023, 18, 583−594

of either kinase alone exhibiting a smaller effect than the double knockout (Figure 3D). Finally, site-directed mutagenesis of the 14 Ser residues to Ala within the SR-rich LKR region (N^{SAmut}) also recapitulated small-molecule-induced condensation of N (Figure S3E), further validating the on-target activity of these compounds. These Wnt pathway and genetic data confirm GSK3 as the target of the small-molecule inhibitors and suggest that GSK3α and GSK3β play partially redundant roles in phosphorylating SARS-CoV-2 N and preventing its condensation, as they do for other proteins that are regulated by GSK3.[33]

ATP-Competitive GSK3 Inhibitors Induce pan-HCoV N Condensate Hardening. GSK3 was previously reported to regulate the condensation of N from SARS-CoV and SARS-CoV-2,[22,24,34,35] but less closely related coronaviruses have not been tested. We thus followed up by treating all seven A549 cell lines expressing N-EGFP from the various human coronaviruses with all seven ATP-competitive GSK3 inhibitors and analyzing N condensation. Robust and reproducible dose-dependent N condensation was observed across all seven Ns (Figures 3E,F and S4A,B and Table S4). These data suggest that regulation of N condensation by GSK3 is conserved among HCoVs, even though the sequences of divergent Ns are only approximately 25% identical. We also found that treatment of N proteins from the bat coronaviruses (bat-CoVs) RaTG13, WIV1, HKU4, HKU10, and HKU8 with the most potent GSK3 inhibitor, LY2090134, induced their phase separation (Figure S4C). Overall, our data indicate that N condensation across all seven HCoVs as well as several bat-CoVs is negatively modulated by GSK3. However, the sensitivity of different HCoV Ns to the pro-condensation effects of GSK3 inhibitors varied considerably (Figure 3F). For example, HCoV-HKU1 and HCoV-NL63 N were much more sensitive to compound modulation than SARS-CoV-2 N, with EC50s for all compounds typically being 1−2 orders of magnitude lower compared to SARS-CoV-2 N, despite similar N expression levels (Figure S1A).

Dephosphorylation of SARS-CoV-2 N by inhibition of GSK3 is thought to promote N phase transition from a liquid-like condensate state to a more gel-like, less dynamic state.[24] We probed the dynamics of various HCoV N condensates in the presence of our most potent GSK3 inhibitor LY2090314, using FRAP. We observed that LY2090314-induced SARS-CoV, SARS-CoV-2, HCoV-OC43, and MERS-CoV N condensates were less dynamic than their corresponding polyIC-induced condensates, with percentage recovery over 2 min decreasing from 53.3/50.5/70.8/72.1% in the polyIC-treated condition to 6.8/13.9/35.6/5.6% in the LY2090314-treated condition, respectively (Figure S4D). LY2090314 treatment did not result in any statistically significant changes in percentage recovery for constitutive HCoV-229E, HCoV-NL63, and HCoV-HKU1 condensates, likely owing to the already slow dynamics of constitutive N condensates. Overall, this suggests that ATP-competitive GSK3 inhibitors are not only capable of inducing N condensation from a basal soluble state, but also result in hardened N condensates with much slower dynamics compared to polyIC-induced N condensates.

GSK3 has been considered as a therapeutic target for the treatment of coronavirus infections,[34−37] but a concern is possible toxicity. For GSK3-targeting inhibitors, the most relevant host pathway to consider for safety is canonical Wnt signaling through β-catenin, which is activated by GSK3 inhibition.[38] This can drive hyperproliferation of epithelial cells in the gut, which is considered a negative safety signal.[39] As a preliminary indicator of therapeutic index, we compared the inhibitor EC50 values obtained in our N condensation assays to EC50s for Wnt pathway activation. In addition to the ATP-competitive GSK3 inhibitors listed above, we also tested two non-ATP-competitive inhibitors (tideglusib, TDZD-8), of which tideglusib has been shown to not activate β-catenin signaling.[40] We found a correlation between the EC50s for N condensation and Wnt signaling activation (via β-catenin activation) for the ATP-competitive inhibitors, with more potent pro-condensation GSK3 inhibitors such as LY2090314 also activating Wnt signaling at lower concentrations (Figure 3F, right). Conversely, the non-ATP-competitive inhibitors were inactive on both assays (Figures 3F and S4A). These data suggest that for HCoVs like SARS-CoV-2, it will be difficult to separate the safety risk of Wnt signaling activation from N modulation since inhibitor concentrations required for N modulation would also activate Wnt signaling. However, therapeutic modulation of N condensation may be viable in the case of HCoVs whose Ns are unusually sensitive to GSK3 inhibition, such as HCoV-NL63 and HCoV-HKU1, where drug exposure below the threshold for activating Wnt signaling might be antiviral.

SARS-CoV-2 N Condensate Inhibitor Screen Identifies Compounds That Inhibit the polyIC Input. Our condensate inhibition screen probed the same compound library. After counter-screening, we identified four hit compounds that robustly reduced the number of polyIC-induced N puncta per cell. These included three compounds annotated as Bcr-Abl/Src inhibitors (bosutinib, ponatinib, and olverembatinib) as well as a plant-derived polyphenol, salvianolic acid B (SalB) (Figure 4A,B and Table S5).

To test if these compounds act directly on N itself, or indirectly via a host factor, we tested whether they inhibited two endogenous pathways that are induced by transfection of polyIC, in particular, SG formation and IRF3 translocation into the nucleus triggered by RIG-I and related viral RNA sensors. Both pathways were measured using cell-based high-content assays. At high concentrations, the three annotated kinase inhibitors (bosutinib, ponatinib, and olverembatinib) inhibited SG formation triggered by polyIC or arsenite, as well as IRF3 nuclear localization triggered by polyIC or cGAMP (Figures 4C and S5A). These data suggest action by polypharmacology. Bosutinib exhibited more potent activity against polyIC-triggered IRF3 translocation, suggesting a possibly interesting off-target activity on that pathway. We also tested two other Bcr-Abl kinase inhibitors (nilotinib, imatinib) and two other Src kinase inhibitors (saracatinib, PP2) in our assay. None of the compounds resulted in robust dose-dependent inhibition of polyIC-induced N condensation (Figure S5B), suggesting that the relevant target(s) may not be Abl or Src family kinases. Interestingly, treatment with nilotinib instead resulted in an increase in N condensation, suggesting an additional possible off-target N condensation mechanism. The polyphenol SalB was more specific, inhibiting only polyIC-induced SG formation and IRF3 nuclear localization (Figures 4C and S5A). Thus, all of the condensate inhibitors act against the polyIC input into the assay, presumably by inhibiting host factors required for polyIC signaling. We suspect the kinase inhibitors block the polyIC input via kinase inhibition, but likely not by inhibition of their annotated primary targets Abl or Src.

https://doi.org/10.1021/acschembio.2c00908
ACS Chem. Biol. 2023, 18, 583−594

A

Class	Compound	Paper	Virus	Cell line
GSK3 inhibitors	LY2090314	Murer et al., 2022	229E	Huh7
			OC43	Huh7
			SARS2	VeroE6
	CHIR-98014	Murer et al., 2022	229E	Huh7
			OC43	Huh7
		Bouhaddou et al., 2020	SARS2	A549-ACE2
	6-BIO	Murer et al., 2022	229E	Huh7
			OC43	Huh7
			SARS2	A549-ACE2
Src/Abl inhibitors	Olverembatinib	Murer et al., 2022	229E	Huh7
			OC43	Huh7
			SARS2	VeroE6
		Patten et al., 2021	SARS2	VeroE6
	Bosutinib	Yang et al., 2021	SARS2	VeroE6
		Xiao et al., 2020	OC43	LLC-MK2
Proteasome inhibitors	Carfilzomib	Patten et al., 2021	SARS2	VeroE6
	Bortezomib	Shen et al., 2022	SARS2	VeroE6
	Ixazomib	Shen et al., 2022	SARS2	VeroE6

B

GSK3 inhibitors	Virus	Antiviral IC50 (μM)	N cond. EC50 (μM)
LY2090314	229E	0.002[a]	0.001
CHIR-98014	229E	0.26[a]	0.2
	SARS2	4.8[b]	1.5
6-BIO	229E	0.46[a]	0.1

[a]Murer et al., 2022
[b]Bouhaddou et al., 2020

>50 EC50 (uM) 0

C

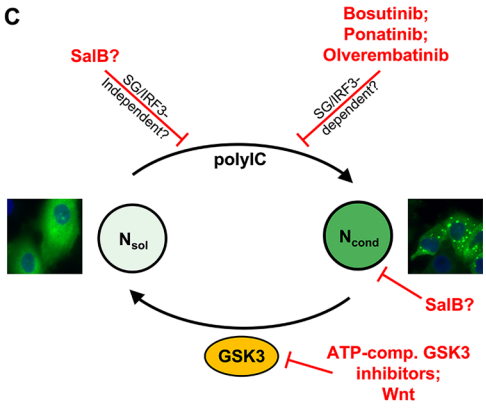

Figure 5. N condensate modulators are antiviral against SARS-CoV-2, HCoV-OC43, and HCoV-229E. (A) Active compounds from our screens and follow-up assays that have been identified as antiviral across various HCoV infection models by prior studies. (B) Antiviral IC50s (from prior studies, where available) and corresponding N condensation EC50s (from our N condensation assays) for GSK3 inhibitors illustrating a correlation between N condensation potency and antiviral activity. (C) Schematic illustrating the tunability of N condensation by small molecules identified in our screens. GSK3 phosphorylates all seven HCoV N proteins. ATP-competitive GSK3 inhibitors and Wnt signaling inhibit N phosphorylation and promote N condensation, with resultant condensates exhibiting significantly reduced dynamics. Inhibition of one or more host factors involved in SG/IRF3 signaling pathways by the Bcr-Abl/Src kinase family of inhibitors prevent polyIC/RNA-induced N condensation. In addition, SalB may inhibit polyIC/RNA-induced N condensation through different mechanisms such as the inhibition of host factor(s) that induce N condensation through SG/IRF3-independent mechanisms, and/or direct interference of N-RNA/polyIC interactions. N_{sol}: soluble N; N_{cond}: condensed N; ATP-comp.: ATP-competitive.

We next sought to determine the species-specificity of the four active condensate inhibitors (bosutinib, ponatinib, olverembatinib, SalB). All four compounds also showed significant suppression of polyIC-induced SARS-CoV/SARS-CoV-2/HCoV-OC43/MERS-CoV N condensation (Figures 4D,E and S5C and Table S6). However, we did not observe significant inhibition of the formation of constitutive HCoV-229E/HCoV-NL63/HCoV-HKU1 N condensates independent of polyIC (Figure S5D and Table S6), further demonstrating that the activity of the condensate inhibitors is polyIC-dependent. No conclusive inhibition of polyIC-induced N condensates could be determined for HCoV-229E/HCoV-NL63/HCoV-HKU1 owing to the relatively small difference in number of N puncta per cell between the polyIC-induced state and basal condensation state (Figure S5E).

Condensate Formation and Antiviral Activity. The library we screened contains approved drugs and well-annotated tool compounds. Similar libraries have been screened by multiple groups for antiviral activity against HCoVs.[41−46] Several of the GSK3, Src/Abl, and proteasome inhibitors we identified as N condensation modulators were previously shown to have antiviral activity. The published data cover several HCoV species and several different cell lines (Figure 5A). In addition, for some of the GSK3 inhibitors, published antiviral IC50s showed correlation with the N condensation EC50s determined here. Notably, the most potent pro-condenser compound LY2090314 also exhibited antiviral activity against HCoV-229E at low inhibitor concentrations (Figure 5B). This suggests that possible on-target activity on N condensation may be responsible for the antiviral activity of the GSK3 inhibitors, and that small-molecule modulation of N condensation can exert antiviral activity.

Discussion. Biomolecular condensates play a role in cellular processes such as embryonic development, stress response and pathological aggregation of proteins, and are also critical for various stages of viral replication. In this study, we show that (A) N condensation is a common phenomenon across all seven HCoVs, and (B) small molecules can promote or inhibit N condensation via perturbation of host targets, and this activity tends to be common across N proteins from all HCoV species tested (Figure 5C). Several of these small molecules are also active against multiple HCoV infection models. These data show that perturbation of viral condensate dynamics via host factors has the potential to generate drugs with antiviral activity across multiple viral species, including new pandemic species. Our approach also illustrates that cell-based screens using viral genes can predict potential antiviral activity of small molecules without requiring access to whole virus infection models.

Our high-content screens identified small-molecule inhibitors of GSK3 that tune both the fraction of condensed N protein as well as the dynamics of N condensates. GSK3 has previously been proposed as a HCoV target.[35−37] Our work reveals its pan-HCoV potential and also highlights the safety risk associated with Wnt pathway activation. GSK3 is an abundant, constitutively active Ser/Thr kinase that phosphor-

https://doi.org/10.1021/acschembio.2c00908
ACS Chem. Biol. 2023, 18, 583−594

ylates a wide range of pre-primed substrates[47] and has previously been shown to phosphorylate both SARS-CoV and SARS-CoV-2 N along its SR-rich LKR region.[22,24,34] In this study, we show that GSK3 inhibitors exhibit the same condensate-modulating effects across all seven HCoV and five bat-CoV N proteins. These condensate-hardening inhibitors likely inhibit viral replication through on-target induction of N condensation/aggregation. In addition, several others have also demonstrated that GSK3 inhibitors are antiviral against various HCoVs.[34,35,41,43] This further promotes GSK3 as a candidate target for the development of multi-CoV antivirals and illustrates one of the major benefits of host-targeting to achieve broad-spectrum antiviral activity (in addition to reduced risk of resistance development). However, as with any host target, a key concern is therapeutic index and toxicity due to perturbation of host pathways that depend on the target, in this case potentially oncogenic β-catenin signaling. For the HCoVs whose Ns are much more sensitive to compound modulation such as HCoV-NL63, it could be that antiviral activity can be achieved with minimal activation of β-catenin signaling in live virus infection models. In addition, a follow-up would be to investigate the molecular basis behind the difference in sensitivity of various Ns to compound modulation. For example, this could be done by determining if dephosphorylation occurs at lower concentrations of GSK3 inhibitors for more sensitive N proteins, or if these N proteins dephosphorylate at similar concentrations of inhibitor but require a lower degree of dephosphorylation to condense. The main SARS-CoV-2 N Ser phosphorylation site identified by mass spectrometry to be perturbed by LY2090314 treatment (Figure S3D) is conserved across all other Ns, with the exception of MERS-CoV, where it is substituted with Thr. It is thus likely that if different phosphorylation states account for the varied responses of N proteins to inhibitors, the important phosphorylation sites may be located within the rest of the Ser-rich LKR region, which was under-represented by mass spectrometry.

Additionally, condensate targets offer novel avenues for optimization chemistry, notably the potential to increase on-target activity by partitioning of the drug into the condensate.[48] Since viral and host condensates have different compositions, this effect should enable improvement of selectivity. We compared EC50 values for nine GSK3 inhibitors in N condensate versus Wnt activation assays and found no compounds that were notably selective for the viral pathway over the host pathway (Figure 3F). Testing a larger library of GSK inhibitors, or a focused medicinal chemistry effort, might tease out selectivity between these pathways.

The N condensate inhibitors we identified appear to target the polyIC input to N condensation, as evidenced by their ability to block induction of polyIC-induced IRF3 translocation and SG assembly. A potentially causal relationship between SG induction and SARS-CoV-2 N condensation has been shown by others.[16,49] The three kinase inhibitors we identified (bosutinib, ponatinib, and olverembatinib) are annotated as targeting Bcr-Abl and Src. However, our investigation of additional potent Bcr-Abl and Src inhibitors failed to support this hypothesis. We currently suspect their activities, especially at concentrations of 1 μM and higher, may be due to polypharmacology that could be resolved by kinase activity profiling and additional structure−activity relationship (SAR).

The polyphenolic natural product SalB represents a class of compounds that has a broad range of biological effects and are not considered promising starts for medicinal chemistry. SalB selectively blocks polyIC input at some stage as evidenced by its inhibition of only polyIC-induced IRF3 activation and SG formation. However, its polypharmacology raises the possibility that it may also act directly on N by physically inhibiting N-RNA or general RNA−protein interactions. It was shown in a previous study that another polyphenol natural product, (−)-gallocatechin gallate, is able to disrupt SARS-CoV-2 N condensation through direct interference of N-RNA binding.[50] Taken together, the condensate inhibitors demonstrate that small molecules are capable of disrupting liquid−liquid phase separation of HCoV N proteins through varied mechanisms.

The use of the FDA-approved library that has been screened several times for antiviral activity allows us to see a potential correlation with condensate formation and virus infectivity. However, one of the limitations of screening with an annotated FDA-approved library is the lack of diversity in pharmacological targets. Screening a larger, more chemically diverse compound library is a natural next step for our approach. Additionally, while our primary goal in screening for modulators of HCoV N condensates was to identify targets for treating COVID-19 and other HCoV infections, our approach is also relevant to other diseases where ribonucleoprotein (RNP) aggregates have been causally implicated. Neurological diseases such as Huntington's disease, spinocerebellar ataxia, and Fragile X syndrome arise from nucleotide repeat expansions in noncoding RNA that give rise to pathological nuclear RNP granules.[51] Similarly, pathological cytoplasmic RNP inclusions of mutant variants of the Fused in sarcoma (FUS) protein are the hallmark of ALS.[52−54] In addition to its role in virus infections, double-stranded RNA signaling may also underly neurodegeneration caused by the *C9ORF72* locus.[55] Taken together, the ability to screen for condensate dynamics as a therapeutic target supports the value of moving forward with larger more diverse compound libraries to reveal novel condensate biology in both viral infections as well as in other indications such as neurological diseases.

MATERIALS AND METHODS

Cell Lines and Cell Culture. HEK293T/17 (CRL-11268) and A549 (CCL-185) cells were purchased from ATCC. BJ-5ta ΔcGAS cells were obtained from Dr. Tai L. Ng (Harvard Medical School). HEK293T/17 cells and BJ-5ta ΔcGAS cells were maintained in Dulbecco's modified Eagle's medium (DMEM; ATCC 30-2002) supplemented with 10% (v/v) fetal bovine serum (FBS; Gibco 10438026), 1000 U mL^{-1} penicillin−streptomycin (Gibco 15140122), and 100 μg mL^{-1} normocin (Invivogen ant-nr-1). Wild-type A549 cells were maintained in F-12K medium (ATCC 30-2004) supplemented with 10% (v/v) FBS, 1000 U mL^{-1} penicillin−streptomycin, and 100 μg mL^{-1} normocin or DMEM supplemented with 10% (v/v) FBS. A549 stable cell lines expressing various HCoV N-EGFP were maintained in full F-12K culture medium with 1.5 μg mL^{-1} puromycin (Gibco A1113803). Cells were maintained at 37 °C and 5% CO_2 in a humidified environment and subcultured twice a week by DPBS washing (Gibco 14190250) followed by trypsinization (Corning MT25053CI) from 90 to 20% confluence.

Fluorescence Recovery after Photobleaching (FRAP). FRAP experiments were performed on a DeltaVision OMX Blaze microscope equipped with a 60×/1.42 Plan Apo oil objective (Olympus), a 488 nm laser, and a PCO edge Front Illuminated sCMOS camera. N-EGFP was imaged with a light-emitting diode (LED), 477/32 nm bandpass filter, and 528/48 nm emission filter. Bleaching of N-EGFP

https://doi.org/10.1021/acschembio.2c00908
ACS Chem. Biol. 2023, 18, 583−594

was performed with a 488 nm laser. For each experimental sample, seven condensates were bleached within a circular region of about 1.2 μm diameter at 31.3% laser transmission for 50 ms. A total of 120 frames were recorded at one frame per 2 s, for a total of 2 min (two frames recorded prior to bleach event, followed by 117 subsequent post-bleach frames). Images were processed in FIJI software (NIH). The fluorescence intensity of a 0.32 μm diameter circular region of interest (ROI) within the bleached spot was monitored over time (I_{bleached}). The fluorescence intensity within the same ROI pre-bleaching ($I_{\text{pre-bleach}}$) and immediately post-bleaching ($I_{\text{post-bleach}}$) were also recorded. The fluorescence intensity of a separate rectangular ROI of 2.72 μm diameter away from one bleached ROI per sample was monitored over time ($I_{\text{background}}$). The FRAP recovery intensities at any given time point (I_t) were calculated as follows

$$I_t = \frac{I_{\text{bleached}} - I_{\text{background}}}{I_{\text{pre-bleached}}}$$

The curves obtained were then normalized as follows

$$\text{normalization} = \frac{I_t - I_{\text{post-bleach}}}{1 - I_{\text{post-bleach}}}$$

The mean and standard deviation of the final normalized values were plotted for seven condensates per experimental condition, and the final normalized recovery value was taken as the percentage recovery for each condition.

High-Content Compound Screening. The primary screen was performed at AbbVie as follows. Briefly, cells were seeded in PerkinElmer LLC ViewPlate 384-well black, optically clear bottom plates at 2000 cells per well and incubated overnight. The FDA-annotated Drug Library from Selleckchem (Selleck 2019) comprising 2554 compounds was added at a final concentration of 10 μM and incubated overnight on duplicate plates. Plates for the condensate inhibition screen were additionally transfected with a final concentration of 1 μg mL^{-1} polyIC 17 h after compound addition to induce N condensation and incubated for a further 7 h. All plates for both the pro-condensation and condensation inhibition screens were fixed with 3% formaldehyde and nuclei stained with Hoechst 33342 for nuclear identification. Plates were scanned on the Thermo Fisher CX7 LZR using a 20× objective and widefield imaging mode. Nuclei staining was imaged with the 405LZR_BGFR_BGFR filter. GFP was imaged with the 488LZR_BGFR_BGFR filter. Images were analyzed with automatic image analysis as described below. The Z' for both the pro-condensation and condensation inhibition assays were calculated as follows

$$Z' = \frac{3(\sigma_{\text{pos}} + \sigma_{\text{neg}})}{|\mu_{\text{pos}} + \mu_{\text{neg}}|}$$

where σ_{pos} is the SD of positive control, σ_{neg} is the SD of negative control (DMSO), μ_{pos} is the mean of positive control, and μ_{neg} is the mean of negative control (DMSO). For visualization of screening data (Figures 3A and 4A), % activity compared to DMSO control was calculated as follows

$$\%\ \text{activity} = \frac{(\text{cMax} - \text{experimental})}{(\text{cMax} - \text{cMin})} \times 100$$

For the pro-condensation screen, cMax = mean number of puncta per cell for positive control MS023 and cMin = mean number of puncta per cell for negative control DMSO. For the condensation inhibition screen, cMax = mean number of puncta per cell for negative control DMSO and cMin = mean number of puncta per cell for positive control salvianolic acid B. Hit triage criteria are detailed in Table S2.

See the Supporting Information for more details on follow-up experiments for hit compounds across all seven A549 HCoV N-EGFP cell lines.

Automatic Image Analysis. Image analysis for the primary screen as well as follow-up experiments were performed at AbbVie and HMS, respectively, with independent image analysis pipelines that demonstrated highly reproducible results. At AbbVie, image analysis was performed using SpotDetector.V4 algorithm (Figure S2A). The output feature SpotCountPerObject was used to evaluate the changes in N protein condensation in both screens. At Harvard Medical School, image analysis for follow-up experiments was performed with Molecular Devices MetaXpress software with customized image analysis pipelines for quantification of N puncta (Figure S2B). For quantification of N puncta upon treatment with the pro-condensation proteasome inhibitors, thresholds for the image analysis pipeline were modified slightly to enable more robust and accurate identification of smaller and dimmer puncta. For dose−response experiments, mean values were fit with a three-parameter curve in Prism (GraphPad 9).

Other Materials and Methods. See Supporting Information for more details.

■ ASSOCIATED CONTENT

Supporting Information

The Supporting Information is available free of charge at https://pubs.acs.org/doi/10.1021/acschembio.2c00908.

Additional materials and methods; sources of compounds/ligands; DNA sequences; supporting figures containing further characterization of N-expressing cell lines, screening methodology schematics, and additional dose−response data for cell-based assays; and raw data files for both screens and dose−response experiments for hit compounds across all seven N-expressing cell lines (PDF)

Pro-condensation screen raw data (Table S3) (XLSX)

Dose-responses for pro-condensation hit compounds across seven HCoV N cell lines (Table S4) (XLSX)

Condensate inhibition screen raw data (Table S5) (XLSX)

Dose-responses for condensate inhibiting hit compounds across seven HCoV N cell lines (Table S6) (XLSX)

■ AUTHOR INFORMATION

Corresponding Authors

Pamela A. Silver − *Department of Systems Biology, Harvard Medical School, Boston, Massachusetts 02115, United States; Wyss Institute for Biologically Inspired Engineering, Harvard University, Boston, Massachusetts 02115, United States;* orcid.org/0000-0002-7856-4071; Email: pamela_silver@hms.harvard.edu

Timothy J. Mitchison − *Department of Systems Biology, Harvard Medical School, Boston, Massachusetts 02115, United States;* Email: timothy_mitchison@hms.harvard.edu

Authors

Rui Tong Quek − *Department of Systems Biology, Harvard Medical School, Boston, Massachusetts 02115, United States; Wyss Institute for Biologically Inspired Engineering, Harvard University, Boston, Massachusetts 02115, United States;* orcid.org/0000-0002-0192-8279

Kierra S. Hardy − *Department of Systems Biology, Harvard Medical School, Boston, Massachusetts 02115, United States; Wyss Institute for Biologically Inspired Engineering, Harvard University, Boston, Massachusetts 02115, United States*

Stephen G. Walker − *Drug Discovery Science and Technology, AbbVie Inc., North Chicago, Illinois 60064, United States*

Dan T. Nguyen − *Department of Systems Biology, Harvard Medical School, Boston, Massachusetts 02115, United States; Wyss Institute for Biologically Inspired Engineering, Harvard*

https://doi.org/10.1021/acschembio.2c00908
ACS Chem. Biol. 2023, 18, 583−594

University, Boston, Massachusetts 02115, United States; orcid.org/0000-0001-8198-9401

Taciani de Almeida Magalhães − *Department of Cell Biology, Harvard Medical School, Boston, Massachusetts 02115, United States*

Adrian Salic − *Department of Cell Biology, Harvard Medical School, Boston, Massachusetts 02115, United States*

Sujatha M. Gopalakrishnan − *Drug Discovery Science and Technology, AbbVie Inc., North Chicago, Illinois 60064, United States*

Complete contact information is available at: https://pubs.acs.org/10.1021/acschembio.2c00908

Notes

The authors declare no competing financial interest.

■ ACKNOWLEDGMENTS

This work was sponsored by a research alliance with AbbVie, Inc. Rui Tong Quek was supported by the Agency for Science, Technology and Research NSS (Ph.D.) predoctoral fellowship. The content and conclusions included in this document are solely those of the authors and do not necessarily represent official views of any funders. The authors thank the Nikon Imaging Center at HMS for help with fluorescence microscopy, the Taplin Mass Spectrometry Facility at HMS for help with mass spectrometry, and the ICCB-Longwood Screening Facility at HMS, in particular C. Yapp for assistance with image analysis and for access to high-throughput screening equipment. The authors also thank T. Ng (HMS) for providing cell lines and plasmids. R.T.Q. and K.S.H. generated cell lines and designed the high-throughput screening assay. S.G.W. performed the high-throughput small-molecule screens and validation of hits. D.T.N. designed custom image analysis pipelines and assisted with image analysis. T.d.A.M. performed the Wnt reporter assays and processed the data. R.T.Q. performed qualitative imaging, follow-up/mechanistic assays, and data analyses, as well as wrote the manuscript. S.M.G., P.A.S., and T.J.M. managed the team, assisted with data analysis and interpretation, and provided scientific insight and advice on writing the paper. AbbVie participated in the study design and execution of experiments including the interpretation of data and review and approval of the publication. AbbVie provided financial support for this research. All authors provided critical feedback for the manuscript.

■ REFERENCES

(1) Boeynaems, S.; Alberti, S.; Fawzi, N. L.; Mittag, T.; Polymenidou, M.; Rousseau, F.; Schymkowitz, J.; Shorter, J.; Wolozin, B.; Van Den Bosch, L.; Tompa, P.; Fuxreiter, M. Protein Phase Separation: A New Phase in Cell Biology. *Trends Cell Biol.* **2018**, *28*, 420−435.

(2) Banani, S. F.; Lee, H. O.; Hyman, A. A.; Rosen, M. K. Biomolecular condensates: organizers of cellular biochemistry. *Nat. Rev. Mol. Cell Biol.* **2017**, *18*, 285−298.

(3) Shin, Y.; Brangwynne, C. P. Liquid phase condensation in cell physiology and disease. *Science* **2017**, *357*, No. eaaf4382.

(4) Zhao, Y. G.; Zhang, H. Phase Separation in Membrane Biology: The Interplay between Membrane-Bound Organelles and Membraneless Condensates. *Dev. Cell* **2020**, *55*, 30−44.

(5) Nikolic, J.; Le Bars, R.; Lama, Z.; Scrima, N.; Lagaudrière-Gesbert, C.; Gaudin, Y.; Blondel, D. Negri bodies are viral factories with properties of liquid organelles. *Nat. Commun.* **2017**, *8*, No. 58.

(6) Heinrich, B. S.; Maliga, Z.; Stein David, A.; Hyman Anthony, A.; Whelan Sean, P. J.; Palese, P. Phase Transitions Drive the Formation of Vesicular Stomatitis Virus Replication Compartments. *mBio* **2018**, *9*, No. e02290-17.

(7) Heinrich, B. S.; Cureton, D. K.; Rahmeh, A. A.; Whelan, S. P. J. Protein expression redirects vesicular stomatitis virus RNA synthesis to cytoplasmic inclusions. *PLoS Pathog.* **2010**, *6*, No. e1000958.

(8) Rincheval, V.; Lelek, M.; Gault, E.; Bouillier, C.; Sitterlin, D.; Blouquit-Laye, S.; Galloux, M.; Zimmer, C.; Eleouet, J.-F.; Rameix-Welti, M.-A. Functional organization of cytoplasmic inclusion bodies in cells infected by respiratory syncytial virus. *Nat. Commun.* **2017**, *8*, No. 563.

(9) Hoenen, T.; Shabman, R. S.; Groseth, A.; Herwig, A.; Weber, M.; Schudt, G.; Dolnik, O.; Basler, C. F.; Becker, S.; Feldmann, H. Inclusion bodies are a site of ebolavirus replication. *J. Virol.* **2012**, *86*, 11779−11788.

(10) Guseva, S.; Milles, S.; Jensen, M. R.; Salvi, N.; Kleman, J.-P.; Maurin, D.; Ruigrok, R. W. H.; Blackledge, M. Measles virus nucleo- and phosphoproteins form liquid-like phase-separated compartments that promote nucleocapsid assembly. *Sci. Adv.* **2020**, *6*, No. eaaz7095.

(11) Carlos, T. S.; Young, D. F.; Schneider, M.; Simas, J. P.; Randall, R. E. Parainfluenza virus 5 genomes are located in viral cytoplasmic bodies whilst the virus dismantles the interferon-induced antiviral state of cells. *J. Gen. Virol.* **2009**, *90*, 2147−2156.

(12) Zhang, S.; Chen, L.; Zhang, G.; Yan, Q.; Yang, X.; Ding, B.; Tang, Q.; Sun, S.; Hu, Z.; Chen, M. An amino acid of human parainfluenza virus type 3 nucleoprotein is critical for template function and cytoplasmic inclusion body formation. *J. Virol.* **2013**, *87*, 12457−12470.

(13) Ringel, M.; Heiner, A.; Behner, L.; Halwe, S.; Sauerhering, L.; Becker, N.; Dietzel, E.; Sawatsky, B.; Kolesnikova, L.; Maisner, A. Nipah virus induces two inclusion body populations: Identification of novel inclusions at the plasma membrane. *PLoS Pathog.* **2019**, *15*, No. e1007733.

(14) Silvestri, L. S.; Taraporewala, Z. F.; Patton, J. T. Rotavirus replication: plus-sense templates for double-stranded RNA synthesis are made in viroplasms. *J. Virol.* **2004**, *78*, 7763−7774.

(15) Nevers, Q.; Albertini, A. A.; Lagaudrière-Gesbert, C.; Gaudin, Y. Negri bodies and other virus membrane-less replication compartments. *Biochim. Biophys. Acta, Mol. Cell Res.* **2020**, *1867*, 118831.

(16) Savastano, A.; Ibáñez de Opakua, A.; Rankovic, M.; Zweckstetter, M. Nucleocapsid protein of SARS-CoV-2 phase separates into RNA-rich polymerase-containing condensates. *Nat. Commun.* **2020**, *11*, No. 6041.

(17) Cong, Y.; Ulasli, M.; Schepers, H.; Mauthe, M.; V'Kovski, P.; Kriegenburg, F.; Thiel, V.; de Haan, C. A. M.; Reggiori, F. Nucleocapsid Protein Recruitment to Replication-Transcription Complexes Plays a Crucial Role in Coronaviral Life Cycle. *J. Virol.* **2020**, *94*, No. e01925-19.

(18) Iserman, C.; Roden, C. A.; Boerneke, M. A.; Sealfon, R. S. G.; McLaughlin, G. A.; Jungreis, I.; Fritch, E. J.; Hou, Y. J.; Ekena, J.; Weidmann, C. A.; Theesfeld, C. L.; Kellis, M.; Troyanskaya, O. G.; Baric, R. S.; Sheahan, T. P.; Weeks, K. M.; Gladfelter, A. S. Genomic RNA Elements Drive Phase Separation of the SARS-CoV-2 Nucleocapsid. *Mol. Cell* **2020**, *80*, 1078.e6−1091.e6.

(19) Chen, H.; Cui, Y.; Han, X.; Hu, W.; Sun, M.; Zhang, Y.; Wang, P.-H.; Song, G.; Chen, W.; Lou, J. Liquid−liquid phase separation by SARS-CoV-2 nucleocapsid protein and RNA. *Cell Res.* **2020**, *30*, 1143−1145.

(20) Cubuk, J.; Alston, J. J.; Incicco, J. J.; Singh, S.; Stuchell-Brereton, M. D.; Ward, M. D.; Zimmerman, M. I.; Vithani, N.; Griffith, D.; Wagoner, J. A.; Bowman, G. R.; Hall, K. B.; Soranno, A.; Holehouse, A. S. The SARS-CoV-2 nucleocapsid protein is dynamic, disordered, and phase separates with RNA. *Nat. Commun.* **2021**, *12*, No. 1936.

(21) Jack, A.; Ferro, L. S.; Trnka, M. J.; Wehri, E.; Nadgir, A.; Nguyenla, X.; Fox, D.; Costa, K.; Stanley, S.; Schaletzky, J.; Yildiz, A. SARS-CoV-2 nucleocapsid protein forms condensates with viral genomic RNA. *PLoS Biol.* **2021**, *19*, No. e3001425.

(22) Lu, S.; Ye, Q.; Singh, D.; Cao, Y.; Diedrich, J. K.; Yates, J. R.; Villa, E.; Cleveland, D. W.; Corbett, K. D. The SARS-CoV-2 nucleocapsid phosphoprotein forms mutually exclusive condensates with RNA and the membrane-associated M protein. *Nat. Commun.* **2021**, *12*, No. 502.
(23) Perdikari, T. M.; Murthy, A. C.; Ryan, V. H.; Watters, S.; Naik, M. T.; Fawzi, N. L. SARS-CoV-2 nucleocapsid protein phase-separates with RNA and with human hnRNPs. *EMBO J.* **2020**, *39*, No. e106478.
(24) Carlson, C. R.; Asfaha, J. B.; Ghent, C. M.; Howard, C. J.; Hartooni, N.; Safari, M.; Frankel, A. D.; Morgan, D. O. Phosphoregulation of Phase Separation by the SARS-CoV-2 N Protein Suggests a Biophysical Basis for its Dual Functions. *Mol. Cell* **2020**, *80*, 1092.e4−1103.e4.
(25) Wheeler, R. J.; Lee, H. O.; Poser, I.; Pal, A.; Doeleman, T.; Kishigami, S.; Kour, S.; Anderson, E. N.; Marrone, L.; Murthy, A. C.; Jahnel, M.; Zhang, X.; Boczek, E.; Fritsch, A.; Fawzi, N. L.; Sterneckert, J.; Pandey, U.; David, D. C.; Davis, B. G.; Baldwin, A. J.; Hermann, A.; Bickle, M.; Alberti, S.; Hyman, A. A. *Small Molecules for Modulating Protein Driven Liquid−Liquid Phase Separation in Treating Neurodegenerative Disease*; bioRxiv, 2019.
(26) Fang, M. Y.; Markmiller, S.; Vu, A. Q.; Javaherian, A.; Dowdle, W. E.; Jolivet, P.; Bushway, P. J.; Castello, N. A.; Baral, A.; Chan, M. Y.; Linsley, J. W.; Linsley, D.; Mercola, M.; Finkbeiner, S.; Lecuyer, E.; Lewcock, J. W.; Yeo, G. W. Small-Molecule Modulation of TDP-43 Recruitment to Stress Granules Prevents Persistent TDP-43 Accumulation in ALS/FTD. *Neuron* **2019**, *103*, 802−819.e811.
(27) Risso-Ballester, J.; Galloux, M.; Cao, J.; Le Goffic, R.; Hontonnou, F.; Jobart-Malfait, A.; Desquesnes, A.; Sake, S. M.; Haid, S.; Du, M.; Zhang, X.; Zhang, H.; Wang, Z.; Rincheval, V.; Zhang, Y.; Pietschmann, T.; Eléouët, J.-F.; Rameix-Welti, M.-A.; Altmeyer, R. A condensate-hardening drug blocks RSV replication in vivo. *Nature* **2021**, *595*, 596−599.
(28) Conti, B. A.; Oppikofer, M. Biomolecular condensates: new opportunities for drug discovery and RNA therapeutics. *Trends Pharmacol. Sci.* **2022**, *43*, 820−837.
(29) Mitrea, D. M.; Mittasch, M.; Gomes, B. F.; Klein, I. A.; Murcko, M. A. Modulating biomolecular condensates: a novel approach to drug discovery. *Nat. Rev. Drug Discovery* **2022**, *21*, 841−862.
(30) Biesaga, M.; Frigolé-Vivas, M.; Salvatella, X. Intrinsically disordered proteins and biomolecular condensates as drug targets. *Curr. Opin. Chem. Biol.* **2021**, *62*, 90−100.
(31) Ishida, T.; Kinoshita, K. PrDOS: prediction of disordered protein regions from amino acid sequence. *Nucleic Acids Res.* **2007**, *35*, W460−W464.
(32) Cai, T.; Yu, Z.; Wang, Z.; Liang, C.; Richard, S. Arginine methylation of SARS-Cov-2 nucleocapsid protein regulates RNA binding, its ability to suppress stress granule formation, and viral replication. *J. Biol. Chem.* **2021**, *297*, No. 100821.
(33) Doble, B. W.; Patel, S.; Wood, G. A.; Kockeritz, L. K.; Woodgett, J. R. Functional redundancy of GSK-3alpha and GSK-3beta in Wnt/beta-catenin signaling shown by using an allelic series of embryonic stem cell lines. *Dev. Cell* **2007**, *12*, 957−971.
(34) Wu, C. H.; Yeh, S. H.; Tsay, Y. G.; Shieh, Y. H.; Kao, C. L.; Chen, Y. S.; Wang, S. H.; Kuo, T. J.; Chen, D. S.; Chen, P. J. Glycogen synthase kinase-3 regulates the phosphorylation of severe acute respiratory syndrome coronavirus nucleocapsid protein and viral replication. *J. Biol. Chem.* **2009**, *284*, 5229−5239.
(35) Liu, X.; Verma, A.; Garcia, G.; Ramage, H.; Lucas, A.; Myers, R. L.; Michaelson, J. J.; Coryell, W.; Kumar, A.; Charney, A. W.; Kazanietz, M. G.; Rader, D. J.; Ritchie, M. D.; Berrettini, W. H.; Schultz, D. C.; Cherry, S.; Damoiseaux, R.; Arumugaswami, V.; Klein, P. S. Targeting the coronavirus nucleocapsid protein through GSK-3 inhibition. *Proc. Natl. Acad. Sci. U.S.A.* **2021**, *118*, No. e2113401118.
(36) Rudd, C. E. GSK-3 Inhibition as a Therapeutic Approach Against SARs CoV2: Dual Benefit of Inhibiting Viral Replication While Potentiating the Immune Response. *Front. Immunol.* **2020**, *11*, No. 1638.
(37) Pillaiyar, T.; Laufer, S. Kinases as Potential Therapeutic Targets for Anti-coronaviral Therapy. *J. Med. Chem.* **2022**, *65*, 955−982.
(38) Wu, D.; Pan, W. GSK3: a multifaceted kinase in Wnt signaling. *Trends Biochem. Sci.* **2010**, *35*, 161−168.
(39) Polakis, P. The oncogenic activation of β-catenin. *Curr. Opin. Genet. Dev.* **1999**, *9*, 15−21.
(40) Martínez-González, L.; Gonzalo-Consuegra, C.; Gómez-Almería, M.; Porras, G.; de Lago, E.; Martín-Requero, Á.; Martínez, A. Tideglusib, a Non-ATP Competitive Inhibitor of GSK-3β as a Drug Candidate for the Treatment of Amyotrophic Lateral Sclerosis. *Int. J. Mol. Sci.* **2021**, *22*, No. 8975.
(41) Murer, L.; Volle, R.; Andriasyan, V.; Petkidis, A.; Gomez-Gonzalez, A.; Yang, L.; Meili, N.; Suomalainen, M.; Bauer, M.; Policarpo Sequeira, D.; Olszewski, D.; Georgi, F.; Kuttler, F.; Turcatti, G.; Greber, U. F. Identification of broad anti-coronavirus chemical agents for repurposing against SARS-CoV-2 and variants of concern. *Curr. Res. Virol. Sci.* **2022**, *3*, No. 100019.
(42) Yang, L.; Pei, R.-j.; Li, H.; Ma, X.-n.; Zhou, Y.; Zhu, F.-h.; He, P.-l.; Tang, W.; Zhang, Y.-c.; Xiong, J.; Xiao, S.-q.; Tong, X.-k.; Zhang, B.; Zuo, J.-p. Identification of SARS-CoV-2 entry inhibitors among already approved drugs. *Acta Pharmacol. Sin.* **2021**, *42*, 1347−1353.
(43) Bouhaddou, M.; Memon, D.; Meyer, B.; White, K. M.; Rezelj, V. V.; Correa Marrero, M.; Polacco, B. J.; Melnyk, J. E.; Ulferts, S.; Kaake, R. M.; Batra, J.; Richards, A. L.; Stevenson, E.; Gordon, D. E.; Rojc, A.; Obernier, K.; Fabius, J. M.; Soucheray, M.; Miorin, L.; Moreno, E.; Koh, C.; Tran, Q. D.; Hardy, A.; Robinot, R.; Vallet, T.; Nilsson-Payant, B. E.; Hernandez-Armenta, C.; Dunham, A.; Weigang, S.; Knerr, J.; Modak, M.; Quintero, D.; Zhou, Y.; Dugourd, A.; Valdeolivas, A.; Patil, T.; Li, Q.; Hüttenhain, R.; Cakir, M.; Muralidharan, M.; Kim, M.; Jang, G.; Tutuncuoglu, B.; Hiatt, J.; Guo, J. Z.; Xu, J.; Bouhaddou, S.; Mathy, C. J. P.; Gaulton, A.; Manners, E. J.; Félix, E.; Shi, Y.; Goff, M.; Lim, J. K.; McBride, T.; O'Neal, M. C.; Cai, Y.; Chang, J. C. J.; Broadhurst, D. J.; Klippsten, S.; De Wit, E.; Leach, A. R.; Kortemme, T.; Shoichet, B.; Ott, M.; Saez-Rodriguez, J.; tenOever, B. R.; Mullins, R. D.; Fischer, E. R.; Kochs, G.; Grosse, R.; García-Sastre, A.; Vignuzzi, M.; Johnson, J. R.; Shokat, K. M.; Swaney, D. L.; Beltrao, P.; Krogan, N. J. The Global Phosphorylation Landscape of SARS-CoV-2 Infection. *Cell* **2020**, *182*, 685.e19−712.e19.
(44) Patten, J. J.; Keiser, P. T.; Gysi, D.; Menichetti, G.; Mori, H.; Donahue, C. J.; Gan, X.; Do Valle, I.; Geoghegan-Barek, K.; Anantpadma, M.; Berrigan, J. L.; Jalloh, S.; Ayazika, T.; Wagner, F.; Zitnik, M.; Ayehunie, S.; Anderson, D.; Loscalzo, J.; Gummuluru, S.; Namchuk, M. N.; Barabasi, A. L.; Davey, R. A.*Multidose Evaluation of 6,710 Drug Repurposing Library Identifies Potent SARS-CoV-2 Infection Inhibitors In Vitro and In Vivo*; bioRxiv, 2021.
(45) Xiao, X.; Wang, C.; Chang, D.; Wang, Y.; Dong, X.; Jiao, T.; Zhao, Z.; Ren, L.; Dela Cruz, C. S.; Sharma, L.; Lei, X.; Wang, J. Identification of Potent and Safe Antiviral Therapeutic Candidates Against SARS-CoV-2. *Front. Immunol.* **2020**, *11*, No. 586572.
(46) Shen, Z.; Halberg, A.; Fong, J. Y.; Guo, J.; Song, G.; Louie, B.; Luedtke, G. R.; Visuthikraisee, V.; Protter, A.; Koh, X.; Baik, T.; Lum, P. Y.*Elucidating Host Cell Response Pathways and Repurposing Therapeutics for SARS-CoV-2 and Other Coronaviruses Using Gene Expression Profiles of Chemical and Genetic Perturbations*; bioRxiv, 2022.
(47) Beurel, E.; Grieco, S. F.; Jope, R. S. Glycogen synthase kinase-3 (GSK3): regulation, actions, and diseases. *Pharmacol. Ther.* **2015**, *148*, 114−131.
(48) Kilgore, H. R.; Young, R. A. Learning the chemical grammar of biomolecular condensates. *Nat. Chem. Biol.* **2022**, *18*, 1298−1304.
(49) Nabeel-Shah, S.; Lee, H.; Ahmed, N.; Burke, G. L.; Farhangmehr, S.; Ashraf, K.; Pu, S.; Braunschweig, U.; Zhong, G.; Wei, H.; Tang, H.; Yang, J.; Marcon, E.; Blencowe, B. J.; Zhang, Z.; Greenblatt, J. F. SARS-CoV-2 nucleocapsid protein binds host mRNAs and attenuates stress granules to impair host stress response. *iScience* **2022**, *25*, No. 103562.
(50) Zhao, M.; Yu, Y.; Sun, L.-M.; Xing, J.-Q.; Li, T.; Zhu, Y.; Wang, M.; Yu, Y.; Xue, W.; Xia, T.; Cai, H.; Han, Q.-Y.; Yin, X.; Li, W.-H.;

Li, A.-L.; Cui, J.; Yuan, Z.; Zhang, R.; Zhou, T.; Zhang, X.-M.; Li, T. GCG inhibits SARS-CoV-2 replication by disrupting the liquid phase condensation of its nucleocapsid protein. *Nat. Commun.* **2021**, *12*, No. 2114.
(51) Zhang, N.; Ashizawa, T. RNA toxicity and foci formation in microsatellite expansion diseases. *Curr. Opin. Genet. Dev.* **2017**, *44*, 17−29.
(52) Shelkovnikova, T. A.; Robinson, H. K.; Southcombe, J. A.; Ninkina, N.; Buchman, V. L. Multistep process of FUS aggregation in the cell cytoplasm involves RNA-dependent and RNA-independent mechanisms. *Hum. Mol. Genet.* **2014**, *23*, 5211−5226.
(53) Kino, Y.; Washizu, C.; Aquilanti, E.; Okuno, M.; Kurosawa, M.; Yamada, M.; Doi, H.; Nukina, N. Intracellular localization and splicing regulation of FUS/TLS are variably affected by amyotrophic lateral sclerosis-linked mutations. *Nucleic Acids Res.* **2011**, *39*, 2781−2798.
(54) Takanashi, K.; Yamaguchi, A. Aggregation of ALS-linked FUS mutant sequesters RNA binding proteins and impairs RNA granules formation. *Biochem. Biophys. Res. Commun.* **2014**, *452*, 600−607.
(55) Rodriguez, S.; Sahin, A.; Schrank, B. R.; Al-Lawati, H.; Costantino, I.; Benz, E.; Fard, D.; Albers, A. D.; Cao, L.; Gomez, A. C.; Evans, K.; Ratti, E.; Cudkowicz, M.; Frosch, M. P.; Talkowski, M.; Sorger, P. K.; Hyman, B. T.; Albers, M. W. Genome-encoded cytoplasmic double-stranded RNAs, found in C9ORF72 ALS-FTD brain, propagate neuronal loss. *Sci. Transl. Med.* **2021**, *13*, No. eaaz4699.

https://doi.org/10.1021/acschembio.2c00908
ACS Chem. Biol. 2023, 18, 583−594